ASEG-PESA 2013
'THE EUREKA MOMENT'
11-14 AUGUST 2013 • MELBOURNE, AUSTRALIA

New approaches to dealing with remanence: magnetic moment analysis using tensor invariants and remote determination of *in situ* magnetisation using a static tensor gradiometer

David A. Clark
CSIRO Materials Science and Engineering & CSIRO Earth Science and Resource Engineering
PO Box 218, Lindfield, NSW 2070, Australia
David.Clark@csiro.au

SUMMARY

Assuming without evidence that magnetic sources are magnetised parallel to the geomagnetic field can seriously mislead interpretation and can result in drill holes missing their targets. I present two new methods for providing information about magnetisation of anomaly sources, independent of the geometry of the causative bodies. The first method is based on analysis of magnetic gradient tensor data. Integral moments of tensor invariants locate the horizontal and vertical centres of magnetisation and estimate the magnetisation direction. The depth estimate allows correction of the integral moments for the finite range of integration, which can accordingly be restricted to the main part of the anomaly. This reduces interference from neighbouring sources. This method provides information on location, total magnetic moment (magnetisation × volume), and magnetisation direction of a compact source, without making any assumptions about its shape.

The second method employs a single combined gradiometer/magnetometer, operating in base station mode within a magnetic anomaly of interest. The response to geomagnetic time variations allows the contributions of induced magnetisation and remanence to the anomaly to be separated. This method allows remote estimation, prior to drilling of (i) the total magnetisation direction of the source, which is a key to accurate modelling (ii) the remanence direction, which can provide geological information such as age of intrusion or alteration, (iii) the Koenigsberger ratio Q, which is indicative of the magnetic mineralogy of the source. If the source is compact, the method also provides a direct indication of the direction to its centroid.

Key words: magnetisation, remanence, tensor invariants, normalised source strength, geomagnetic variations

INTRODUCTION

A major source of ambiguity in interpretation of magnetic survey data lies in the fact that the physical property contrast that produces the observed magnetic anomalies is a vector, the magnetisation, which may in principle have any orientation. In the absence of independent information about source magnetisation, magnetic modelling usually proceeds on the assumption that the source is magnetised parallel to the local geomagnetic field. However, if the source magnetisation direction differs significantly from the present field direction, due to remanent magnetisation or strong anisotropy, models that fit the data may be grossly in error. For example, interpreted dips of sheet-like bodies and plunges and locations of pipes will be erroneous, with serious consequences for drill targeting. For highly magnetic sources, self-demagnetisation effects may cause similar problems.

This paper presents two methods for analysis of individual magnetic anomalies that allow remote estimation of source magnetisation, while making minimal assumptions about source geometry. The first method relies on integral moments, calculated over a measurement plane, of tensor invariants. These invariants are calculated from magnetic gradient tensor data, which can be either measured directly or derived from high quality conventional magnetic surveys through Fourier filtering or equivalent source techniques.

The integral moments yield estimates of the horizontal and vertical location of the source centroid, the total magnetic moment (magnetisation × volume), and the magnetisation direction. Although integral moment methods are based on integrals calculated over the entire horizontal plane, the centroid depth estimate can be corrected for the finite radius of integration. Once this depth is known, the integral moments of vector and tensor components, as used in Helbig (1963) analysis and its offshoots, can also be accurately corrected for the finite radius of integration, allowing numerical integrations to be confined to the main part of the anomaly, thereby reducing contamination of the integral moments by neighbouring sources and greatly improving parameter estimation.

Provided the area of integration extends well beyond the horizontal dimensions of the source, and the source can be assumed to be depth limited, with bottom depth comparable to the radius of integration or smaller, integral moment methods are in principle independent of source geometry. With the above caveats, estimated parameters are quite robust and do not depend on assumptions about source shape and size. The method is sensitive, however, to erroneous base levels in the vector and tensor components, and to regional trends, which must be removed before applying the method.

The second method is a variant of the differential vector magnetometry (DVM) approach of Clark et al. (1998), which is only now becoming feasible due to improving sensor technology. The original DVM method employs two carefully aligned vector magnetometers, operating in base station mode, with one placed within a magnetic anomaly of interest and the other outside the anomaly to monitor unperturbed geomagnetic time variations. The new method replaces the two vector magnetometers with a single gradiometer plus magnetometer package, placed within an anomaly of interest. The response to geomagnetic time variations allows the contributions of induced magnetisation and remanence to the anomaly to be separated. This method allows remote estimation, prior to drilling of (i) the total magnetisation direction of the source, which is a key to accurate modelling (ii) the remanence direction, which can provide geological information such as age of intrusion or alteration, (iii) the Koenigsberger ratio Q, which is indicative of the magnetic mineralogy of the source. If the source is compact, the method also provides a direct indication of the direction to its centroid.

With current measurement capabilities the modified DVM method can be applied to anomalies for which contribution of induced magnetisation to the anomalous field and gradient is sufficiently large (>100 nT and > 1 pT/m respectively), by monitoring geomagnetic time variations (diurnal, pulsations, substorms etc.) of tens of nT. Given an adequate signal-to-noise ratio, the estimated magnetic properties are completely independent of any assumptions about source geometry, including bodies of effectively infinite depth extent. Thus this method can in principle resolve pathological cases of ambiguity associated with 2D dipping sheets and axially magnetised plunging pipes of great depth extent.

METHOD I: INTEGRAL MOMENTS OF TENSOR INVARIANTS AND COMPONENTS

Helbig (1963) showed that it was possible in principle to determine the magnetic moment vector of an arbitrary finite source by calculating various integral moments of magnetic vector components over an entire horizontal plane above the source. This method was largely neglected over subsequent decades, probably because vector data were rarely available. Schmidt and Clark (1997, 1998) revived the method, with some modifications, by applying it to vector components calculated by Fourier processing of a conventional TMI survey. Since then, a number of researchers, including Phillips (2005), Li et al. (2004), Foss (2006), and Caratori Tontini and Pedersen (2008), have developed and applied this concept. Phillips et al. (2007) extended the analysis to integral moments of the magnetic gradient tensor.

Consider an isolated source with magnetisation **M**, which produces an anomalous field vector **b**. The anomalous magnetic gradient tensor **B** is a symmetric traceless second order tensor (Pedersen and Rasmussen, 1990) given by the vector gradient of **b**. Rotational invariants of the tensor, such as the canonical invariants I_1, I_2 of Pedersen and Rasmussen (1990), can always be expressed in terms of the eigenvalues of the tensor. The normalised source strength (NSS) μ is a particularly useful invariant, because it is completely independent of magnetisation direction for a number of simple, but useful source types: spheres, compact sources that can be represented by a dipole, axially magnetised thin pipes, and 2D sources of arbitrary shape (Beiki et al. 2012; Clark, 2012a,b,c), and is only weakly dependent on magnetisation direction for 3D sources in general (Pilkington and Beiki, 2012). The NSS is defined by

$$\mu = \sqrt{-\lambda_2^2 - \lambda_1\lambda_3}, \tag{1}$$

where $\lambda_1 \geq \lambda_2 \geq \lambda_3$ are the eigenvalues of the tensor in nonincreasing order, which sum to zero due to the tracelessness of the tensor. For a dipole source at (x_0, y_0, h) the NSS takes the simple form

$$\mu = \frac{3Cm}{r^4} = \frac{3Cm}{[(x-x_0)^2 + (y-_0)^2 + h^2]^2}, \tag{2}$$

where $C = \mu_0/4\pi$, m is the magnitude of the magnetic moment **m** and r is the distance from the dipole to the measurement point (x,y,0). Clearly from equation 2, the NSS measured over a plane peaks directly over a dipole source (where r is a minimum) and is independent of orientation of **m**. The depth of the dipole is simply related to the halfwidth of the NSS anomaly. This suggests that measurements of μ over a plane can provide robust estimates of dipole location, unaffected by magnetisation direction.

The intermediate eigenvalue λ_2 for a dipole source is given by Clark (2012b) as

$$\lambda_2 = \mu\cos\phi = \frac{3C\mathbf{m}.\hat{\mathbf{r}}}{r^4}, \tag{3}$$

where ϕ is the angle between the magnetic moment vector and the displacement vector **r** from the dipole to the observation point. Equation 3 shows that λ_2 depends on the orientation of the moment, and therefore can provide information about the magnetisation direction.

The horizontal location (x_0, y_0) of the centre of magnetisation can be estimated from first integral moments of μ or μ^2:

$$x_0 = \frac{\int_{-\infty}^{+\infty}\int_{-\infty}^{+\infty} x\mu\,dxdy}{\int_{-\infty}^{+\infty}\int_{-\infty}^{+\infty} \mu\,dxdy} = \frac{\int_{-\infty}^{+\infty}\int_{-\infty}^{+\infty} x\mu^2\,dxdy}{\int_{-\infty}^{+\infty}\int_{-\infty}^{+\infty} \mu^2\,dxdy}, \tag{4}$$

$$y_0 = \frac{\int_{-\infty}^{+\infty}\int_{-\infty}^{+\infty} y\mu\,dxdy}{\int_{-\infty}^{+\infty}\int_{-\infty}^{+\infty} \mu\,dxdy} = \frac{\int_{-\infty}^{+\infty}\int_{-\infty}^{+\infty} y\mu^2\,dxdy}{\int_{-\infty}^{+\infty}\int_{-\infty}^{+\infty} \mu^2\,dxdy}. \tag{5}$$

In practice the numerical integration is carried out over a finite area to obtain initial estimates of (x_0, y_0). The area of integration is then centred on this point and the integrals recalculated to make any necessary small corrections to the location, which is subsequently used as the origin of coordinates for calculation of all other integral moments. The depth of the centre of magnetisation, h, can be found from

$$h = \frac{\int_{-\infty}^{+\infty}\int_{-\infty}^{+\infty} \mu\,dxdy}{\left[3\pi\int_{-\infty}^{+\infty}\int_{-\infty}^{+\infty} \mu^2\,dxdy\right]^{1/2}}, \tag{6}$$

The magnitude of the magnetic moment, m, is given by

$$m = \frac{\left[\int_{-\infty}^{+\infty}\int_{-\infty}^{+\infty} \mu dxdy\right]^3}{9\pi^2 C \int_{-\infty}^{+\infty}\int_{-\infty}^{+\infty} \mu^2 dxdy}. \quad (7)$$

Equations 4-7 are exact for a point dipole source, which is equivalent to a uniformly magnetised sphere, and is also very accurate for compact sources of arbitrary shape and for fairly equidimensional sources buried at moderate depths, for which the dipole contribution dominates the anomaly. The horizontal location of the centre of magnetisation is also well estimated, even for sources of complex geometry, due to the high centricity of the NSS over arbitrary 3D sources (Pilkington and Beiki, 2012). The depth of the centre of magnetisation can be expected to be reasonably accurate, provided the depth extent of the source is smaller than the radius of integration.

Corrections of the calculated integrals for the finite ranges of x and y are necessary to account for the tails of the anomaly, which are buried in noise, obscured by interfering anomalies or may lie outside the survey area. The first step is to correct the initial estimated depth of the centroid, h', obtained from equation 6 when the integration is perfomed over a disc of radius R:

$$h' = \frac{\iint_{\rho<R} \mu \rho d\rho d\vartheta}{\left[3\pi \iint_{\rho<R} \mu^2 \rho d\rho d\vartheta\right]^{1/2}} = R\sqrt{\frac{1+(R/h)^2}{3+3(R/h)^2+(R/h)^4}}. \quad (8)$$

In equation 8 ρ and ϑ are polar coordinates centred on (x_0, y_0). Solving equation 8 for the true depth h in terms of the known quantities R and h' gives

$$h = h'\sqrt{\frac{2}{1-3(h'/R)^2+\sqrt{1-2(h'/R)^2-3(h'/R)^4}}}. \quad (9)$$

Once the true depth of the centroid has been estimated, all other integral moments used in the subsequent analysis can be corrected for the finite area of integration using analytic integrals based on the theoretical fall-off rate of a point dipole anomaly, as done for conventional Helbig analysis by Schmidt and Clark (1998) and Caratori Tontini and Pedersen (2008).

While it is often more convenient to carry out 2D integrations over square or rectangular areas, rather than discs, it turns out that the corrections for finite discs and for squares of equivalent area (with side $X = R\sqrt{\pi}$) are almost identical for the integral moments of interest, differing by at most about 1% over a wide range of R/h. Therefore the corrections based on discs of integration, which are much easier to calculate, can be used, even though the integrations are performed using square windows.

The corrected magnitude of the magnetic moment, based on the initial estimate m' is

$$m = m'[1+3(h/R)^2+3(h/R)^4]. \quad (10)$$

The corrected components of the magnetic moment $\mathbf{m} = (m_x, m_y, m_z)$ are given by

$$m_x = \frac{h}{2\pi C}\int_{-\infty}^{+\infty}\int_{-\infty}^{+\infty}(x-x_0)\lambda_2 dxdy = \frac{h}{2\pi C}\frac{\int_0^{2\pi}\int_0^R (x-x_0)\lambda_2 \rho d\rho d\theta}{1-\frac{1+3R^2/2h^2}{\left(1+R^2/h^2\right)^{3/2}}}, \quad (11)$$

$$m_y = \frac{h}{2\pi C}\int_{-\infty}^{+\infty}\int_{-\infty}^{+\infty}(y-y_0)\lambda_2 dxdy = \frac{h}{2\pi C}\frac{\int_0^{2\pi}\int_0^R (y-y_0)\lambda_2 \rho d\rho d\theta}{1-\frac{1+3R^2/2h^2}{\left(1+R^2/h^2\right)^{3/2}}}, \quad (12)$$

$$m_z = -\frac{h^2}{2\pi C}\int_{-\infty}^{+\infty}\int_{-\infty}^{+\infty}\lambda_2 dxdy = -\frac{h^2}{2\pi C}\frac{\int_0^{2\pi}\int_0^R \lambda_2 \rho d\rho d\theta}{\left[1-\frac{1}{\left(1+R^2/h^2\right)^{3/2}}\right]}, \quad (13)$$

Note that the declination of the magnetisation, given by dec = atan2(m_x,m_y), is independent of the radius of integration (provided the integral is centred correctly above the source). On the other hand, the inclination of the magnetisation, given by $I = \sin^{-1}(m_z/m)$, requires a correction for the finite range of integration.

METHOD I: FIELD EXAMPLE

The methodology outlined in the previous section has been applied to analysis of publicly available aeromagnetic data from northern NSW, over the southern part of the Thompson Fold Belt. Anomalies over inferred intrusions, corresponding to four prominent discrete equidimensional anomalies within a relatively subdued background field, have been studied in detail. Pratt et al. (2012) modelled the sources of these anomalies, which they labelled Pipes A-D, and estimated magnetisations of the causative bodies. The northern pair of pipes are clearly reversely magnetised (Figure 1), indicating that their magnetisations are dominated by reverse polarity remanence, whereas the southern pair of anomalies (Figure 2) have magnetisations of normal polarity, making the presence of remanence less obvious. However, detailed analysis of these latter anomalies shows that their magnetisations are somewhat oblique to the present field direction, showing that remanence also contributes to the total magnetisation of these bodies.

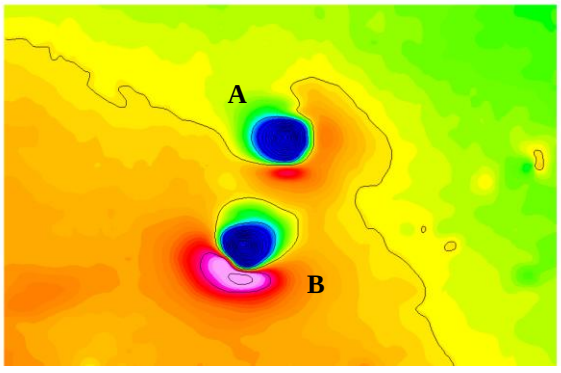

Figure 1. TMI anomalies over the northern pair of pipes (A & B of Pratt et al. (2012)), showing evident reversed polarity. Normalised colour stretch, contour interval is 25 nT.

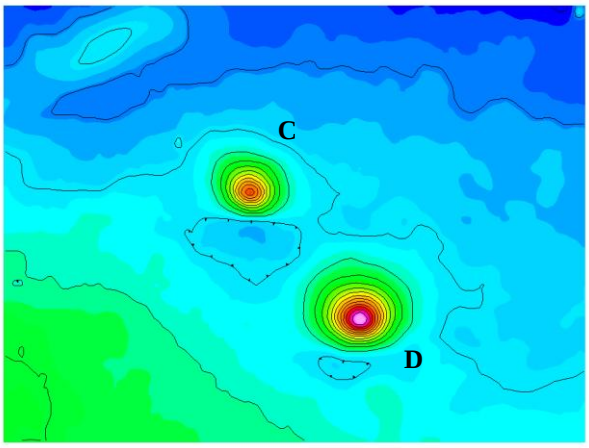

Figure 2. TMI anomalies over the southern pair of pipes (C & D of Pratt et al. (2012)), showing subtle signs of normal polarity magnetisation steeper than the present field. Linear colour stretch, contour interval is 10 nT.

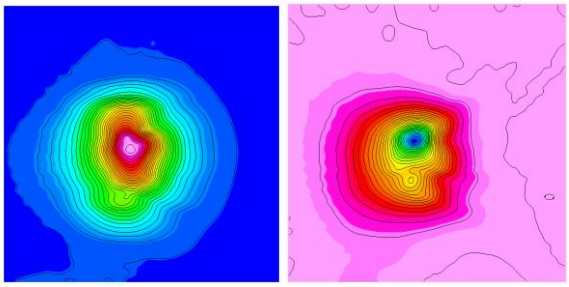

Figure 3. Tensor invariants over Pipe A. LHS is the NSS μ, RHS is the intermediate eigenvalue λ_2. Contour inteval for both is 50 pT/m.

Vector and gradient tensor components were calculated from the gridded TMI data by Fourier filtering, as described by Schmidt and Clark (1998). Grids of tensor invariants were then calculated from the tensor elements. Figure 3 shows images of the invariants μ and λ_2 over the northernmost anomaly (Pipe A). The NSS is almost radially symmetric and lies within a very quiet background, implying that the source is isolated and compact, with minimal interference from neighbouring anomalies, hence it is ideal for application of Helbig-type analyses. NSS anomalies for the other pipes are qualitatively very similar. The centroid of the source is inferred to lie directly beneath the centre of the NSS anomaly. The negative sign of the λ_2 anomaly indicates that the magnetisation is reversed and its slight asymmetry suggests that the magnetisation is steep, but slightly off vertical.

Source centroid locations and magnetic moments were calculated using equations (4)-(13) for each of the four anomalies. The results were then compared with parameters obtained using several other methods:

A. conventional Helbig analysis based on integral moments of vector components,
B. Helbig-type analysis of gradient tensor elements, following Phillips et al. (2007),
C. point-by-point inversion of the anomalous vectors and tensors as described by Clark et al. (2009) and Clark (2012a,b),
D. quadratic regressions of $1/\sqrt{\mu}$ versus x and y, which from equation 2, yield estimates of x_0, y_0, h, m.
E. linear regressions of $1/\sqrt{\mu}$ versus x, y, and $\rho^2 = x^2+y^2$ which from equation 2, yield radially averaged estimates of x_0, y_0, h, m.
F. source location based on the vector gradient of the NSS (Clark, 2012b)
G. the inversion results of Pratt et al. (2012).

Table 1 summarises the results obtained for the four pipes using method I of the previous section.

Table 1. Inverted parameters for Pipes A-D using Method I

Parameter	PIPE A	PIPE B	PIPE C	PIPE D
x_0 (mN)	6693498	6691678	6675979	6673529
y_0 (mE)	476931	476293	504074	505905
h (m)	312	287	547	741
m (Am²)	1.09×10^8	1.06×10^8	1.34×10^8	3.88×10^8
m_x (Am²)	2.42×10^6	-2.54×10^7	2.57×10^7	1.31×10^7
m_y (Am²)	2.77×10^7	-5.39×10^6	3.38×10^6	2.55×10^7
m_z (Am²)	7.42×10^7	7.43×10^7	-9.84×10^7	-2.83×10^8
m* (Am²)	7.92×10^7	7.84×10^7	1.02×10^8	2.84×10^8
Dec (°)	85.0	192.4	7.5	62.8
Inc (°)	+69.5	+71.4	–75.2	–84.2

*magnitude of moment calculated from components of m

Table 2 compares magnetisation directions obtained using method I, methods A-C and the inversion results (G). All the other methods give quite good agreement with the directions from the inversion model, which are assumed to be accurate due to the good fits to the data and the palaeomagnetic plausibility of the results. Directions from tensor Helbig analysis (method C) are inherently insensitive to the radius of integration and agree particularly well with the inversion results, but accurate estimates of moment magnitudes depeneds on a substantial correction that requires accurate estimation of h using method I. Caratori Tontini and Pedersen (2008) suggested a method for estimating the centre of magnetisation from second order integral moments of vector components, but it fails to estimate depths correctly for this data set, possibly because of the steepness of the magnetisations and the large corrections required for finite integration area because of the slow fall-off of the integrands.

All methods indicate moments of about 10^8 Am² for pipes A-C and a somewhat larger moment, ~3 $\times10^8$ Am², for pipe D. Methods C-F, which directly estimate source location are in good agreement for both horizontal location and depth. Table 3 compares magnetic moment and depth estimates for all pipes. Note that Pratt et al. (2012) give depths to the tops of the modelled pipes, not depths to centroids. Twice the difference between the two depths may give an indication of the depth extent of the pipes.

METHOD II: USING A STATIC GRADIOMETER TO DETERMINE MAGNETISATION

The second method presented here extends the theory given by Clark et al. (1998) to exploit the sensitivity of SQUID-based magnetometers and gradiometers to detect local perturbations of anomalies associated with time-varying magnetisation induced by geomagnetic variations. Figure 4 illustrates the principle of the method. Clark et al. (1998) showed that the anomalous field vector **b**, measured at a fixed location within the anomaly, is related to the source magnetisation vector **J** by the matrix equation

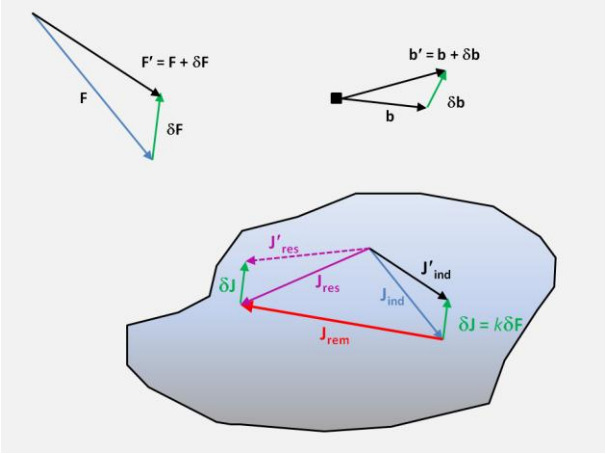

Figure 4. Principle of remote determination of *in* situ magnetic properties. The regional geomagnetic field F undergoes a fluctuation δF, which perturbs the induced magnetisation $\mathbf{J}_{ind}$, but does not affect the contribution of remanence $\mathbf{J}_{rem}$ to the resultant magnetisation $\mathbf{J}_{res}$. The change in source magnetisation produces a change in the observed field and its gradient within the anomaly.

$$\mathbf{b} = \mathbf{A}\mathbf{J}, \tag{14}$$

where **A** is the second order gradient tensor of the pseudo-gravitational potential. The susceptibility is assumed to be isotropic and the magnetisation of the source is assumed to be uniform, at least in direction. **A** depends on the geometry and location of the source, but is independent of the magnetisation. A geomagnetic variation δ**F** produces a change δ**J** = *k*δ**F** in the induced magnetisation, which also equals the change in the resultant magnetisation $\mathbf{J}_{res}$, because the remanence is unaffected. This in turn produces a change in the anomalous field and its gradient. By continuously monitoring geomagnetic variations and gradient perturbations the contributions of induced and remanent magnetisations can be separated. Fluctuations in the vertical gradients of **b**, for example, are given by

$$\delta\left(\frac{\partial \mathbf{b}}{\partial z}\right) = \frac{\partial \mathbf{A}}{\partial z}\delta\mathbf{J} = k\frac{\partial \mathbf{A}}{\partial z}\delta\mathbf{F}. \tag{15}$$

Time series of the gradients and δ**F** yield least squares estimates of the elements of $k\partial\mathbf{A}/\partial z$. The resultant magnetisation of the source, divided by the unknown susceptibility, can then obtained by inverting the relationship, analogous to equation (14), between the gradient anomaly and the resultant magnetisation

$$\mathbf{J}_{res}/k = \left(k\frac{\partial \mathbf{A}}{\partial z}\right)^{-1}\frac{\partial \mathbf{b}}{\partial z}. \tag{16}$$

Equation (16) determines the direction of the resultant magnetisation, which is crucial information for accurate modelling, but not its absolute magnitude. Similar analysis of the orthogonal gradients provides data redundancy, allowing consistency checks and improving error estimates. Because the direction of the induced magnetisation is known, the direction of remanence and the Koenisberger ratio *Q* can also be calculated, using

$$(\mathbf{J}_{rem}/k) = (\mathbf{J}_{res}/k) - \mathbf{F}, \tag{17}$$

$$Q = |\mathbf{J}_{rem}|/kF = |\mathbf{J}_{rem}/k|/F. \tag{18}$$

As noted by Clark et al. (1998) eigenvector analysis of the matrix **A** (or its derivatives) can also provide a direct indication of the direction towards the centroid of a compact source.

The original differential vector magnetometry method trialled by Clark et al. (1998) required two sensitive vector magnetometers, separated by hundreds of metres and aligned to within seconds of arc. The method proposed here requires only a single rigidly mounted package containing a vector magnetometer and gradiometer, that can be placed anywhere within the anomaly and monitored over several hours to allow sufficient geomagnetic field variation. The Superconductivity and Magnetism Group at CSIRO Materials Science and Engineering is adapting a sensitive high-temperature SQUID magnetometer and tensor gradiometer package with gradient sensitivity of about 2 pT/m, developed for underwater UXO detection (Young et al., 2010), for this purpose. Field trials using this instrument are planned for April 2013.

CONCLUSIONS

Value can be added to existing high quality TMI surveys by calculating vector and tensor components and using methods developed for analysis of these types of data, although direct measurement of the gradient tensor is optimal (Clark, 2012a,b,c). For relatively isolated anomalies, analysis of integral moments of tensor invariants, particularly the normalised source strength and the intermediate eigenvalue (method I), provides useful information on source location, direction of magnetisation and total magnetic moment, even when the numerical integrations are restricted to the main portion of the anomaly. The horizontal location of the centre of magnetisation is very robust, particularly when determined from the first integral moment of μ^2, and for compact sources the depth of the centroid can be reliably estimated when a correction for the finite radius of integration is made. The centroid depth is not only important in its own right, but is a crucial parameter for applying corrections to Helbig-type analyses of vector and tensor components, which are in principle independent of source shape (for finite sources).

Magnetic moment vectors estimated using method I and other Helbig-type analyses yield directions of the resultant magnetisation (remanent plus induced), which is crucial for accurate modelling, and give an indication of the size of the source, when plausible magnetisation intensities are assumed.

Method I, like all Helbig-type analyses, is not applicable to sources of great depth extent relative to the resolvable width of the anomaly. Vertical pipe-like bodies, not necessarily narrow or equidimensional, can be analysed by applying these methods to vertical derivatives of the field and/or tensor components and invariants derived from them (Clark, 2012b).
Method II uses time series of vector and gradient measurements to determine the following properties w*ithout making any assumptions about source geometry or location*:

1. direction of total magnetisation (required for accurate modelling; eliminates most ambiguity),

2. direction of remanence, which provides useful geological information such as age of formation or alteration,
3. Koenigsberger ratio Q, which gives information on the magnetic mineralogy of the source,
4. total magnetic moment of a compact source, which is analogous to the total anomalous mass inferred from a gravity anomaly and can indicate probable size of the source for plausible magnetisation strengths,
5. a direct indication of direction to a compact source, which can be used to site initial drill holes,
6. depth and horizontal location of the centroid of a compact source from two stations, occupied simultaneously or consecutively.

Points 1-4 can assist prioritisation of targets prior to drilling and points 1 and 4-6 aid in drill targeting. Method II is not restricted to sources of limited depth extent, allowing it to resolve pathological cases of ambiguity associated with 2D dipping sheets and axially magnetised plunging pipes of great depth extent. However, for sources of great strike extent that are effectively 2D, only the components of magnetisation in the plane normal to strike (which are the only contributors to the observed anomaly) can be determined.

ACKNOWLEDGMENTS

I thank Clive Foss for providing grids of vector and tensor components over the Brewarrina survey pipes. Clive Foss, Dean Hillan and Keith Leslie reviewed the manuscript. This work represents a contribution to research for a PhD at Macquarie University, under the supervision of Drs Mark Lackie and Richard Flood.

REFERENCES

Beiki, M., Clark, D.A., Austin, J.R. and Foss, C.A., 2012a, Estimating source location using normalized magnetic source strength calculated from magnetic gradient tensor data: Geophysics, **77**(6), J23-J37.

Caratori Tontini, F. and Pedersen, L.B., 2008, Interpreting magnetic data by integral moments: Geophysical Journal International, **174**, 815-824.

Clark, D.A., 2012a, New methods for interpretation of magnetic gradient tensor data: ASEG 22nd International Geophysical Conference and Exhibition, 26-29 February 2012, Brisbane, Australia, Expanded Abstracts, 11p.

Clark, D.A., 2012b, New methods for interpretation of magnetic vector and gradient tensor data I: eigenvector analysis and the normalised source strength: Exploration Geophysics, **43**, 267-282, doi:10.1071/EG12020.

Clark, D.A., 2012c, Interpretation of the magnetic gradient tensor and normalized source strength applied to the Tallawang magnetite skarn deposit, New South Wales, Australia: Society of Exploration Geophysicists Annual Meeting, Las Vegas, Expanded Abstracts, 4p.

Clark, D.A., Schmidt, P.W., Coward, D.A. and Huddleston, M.P., 1998. Remote determination of magnetic properties and improved drill targeting of magnetic anomaly sources by Differential Vector Magnetometry (DVM): Exploration Geophysics, 29, 312-319.

Clark, D.A., Young, J.A. and Schmidt, P.W., 2009, Magnetic Tensor Gradiometry in the Marine Environment: Correction of Electric And Magnetic Field And Gradient Measurements in a Conductive Medium and Improved Methods for Magnetic Target Location Using the Magnetic Gradient Tensor: MARELEC (Marine Electromagnetics) Conference, Stockholm, July, 2009, 10p.

Foss, C., 2006. Strategies to manage remanence effects in magnetic inversion. SEG Expanded Abstracts, 25, 938-942.

Helbig, K., 1963. Some integrals of magnetic anomalies and their relation to the parameters of the disturbing body: Zeitschrift für Geophysik, 29, 83-96.

Li, Y., Shearer, S., Haney, M. and Dannemiler, N., 2004. Comprehensive approaches to the inversion of magnetic data with strong remanent magnetization: SEG Expanded Abstracts, 23, 1191-1194.

Pedersen, L.B. and Rasmussen, T.M., 1990. The gradient tensor of potential field anomalies: Some implications on data collection and data processing of maps: Geophysics, 55, 1558-1566.

Phillips, J.D., 2005. Can we estimate total magnetization directions from aeromagnetic data using Helbig's integrals?: Earth Planets Space, 57, 681-689.

Phillips, J.D., Nabighian, M.N., Smith, D.V. and Li, Y., 2007. Estimating locations and total magnetization vectors of compact magnetic sources through combined Helbig and Euler analysis: SEG Expanded Abstracts, 26, 770-774.

Pilkington, M. and Beiki, M., 2012. Mitigating remanent magnetization effects in magnetic data using the normalized source strength. SEG Technical Program Expanded Abstracts 2012, 4p.

Pratt, D.A., McKenzie, K.B. and White, A.S., 2012. The remote determination of magnetic remanence. ASEG 22nd International Geophysical Conference and Exhibition, 26-29 February 2012, Brisbane, Australia, Expanded Abstracts, 5p.

Schmidt, P.W. and Clark, D.A., 1997. Directions of magnetization and vector anomalies derived from total field surveys. Preview, 70, 30-32.

Schmidt, P.W. and Clark, D.A., 1998. The calculation of magnetic components and moments from TMI: A case history from the Tuckers igneous complex, Queensland. Exploration Geophysics, 29, 609-614.

Young, J.A., S.T. Keenan, D.A. Clark, K.E. Leslie, P. Sullivan, P. Fairman, C. Williams, C.P. Foley and S.D. Billings, 2010. A Superconducting Magnetic Tensor Gradiometer for Underwater UXO Detection [Extended Abstract]: 21st International Geophysical Conference & Exhibition (ASEG-PESA 2010); Sydney, 4p.

Table 2. Directions of resultant magnetisation of northern NSW pipes obtained using different methods

Method	Direction of magnetisation: dec°, inc°; (angular difference from inversion result °)			
	PIPE A	**PIPE B**	**PIPE C**	**PIPE D**
Method I (this paper)	85.0, +69.5; (12.6)	192.4, +71.4; (11.4)	7.5, –75.2; (7.6)	62.8, –84.2; (10.8)
A (vector Helbig)	58.6, +65.0; (4.8)	219.5, +58.1; (15.4)	226.9, –83.3; (19.9)	219.5, –78.2; (15.5)
B (tensor Helbig)	60.7, +63.4; (3.0)	222.9, +64.2; (9.1)	349.2, –80.6; (7.3)	332.2, –83.6; (2.1)
C (vector-tensor invers.)	60.8, +71.6; (11)	208.6, +61.8; (13.6)	350.4, –70.9; (4.3)	344.8, –83.7; (3.3)
G (inversion model)	63.3, +60.5; (0)	229.6, +73.0; (0)	337.2, –74.1; (0)	321.5, –82.0; (0)

Table 3. Magnetic moment and depth estimates for northern NSW pipes obtained using different methods

Method	**PIPE A** ***m*** **(Am²);** ***h*** **(m)**	**PIPE B** ***m*** **(Am²);** ***h*** **(m)**	**PIPE C** ***m*** **(Am²);** ***h*** **(m)**	**PIPE D** ***m*** **(Am²);** ***h*** **(m)**
Method I (this paper)	$9.4 \pm 1.5 \times 10^7$; 312	$9.2 \pm 1.4 \times 10^7$; 287	$1.02 \pm 0.16 \times 10^8$; 547	$2.84 \pm 0.52 \times 10^8$; 741
A (vector Helbig)	9.2×10^7; -	9.2×10^7; -	1.2×10^8; -	3.2×10^8; -
B (tensor Helbig)	9.9×10^7; -	9.0×10^7; -	1.0×10^8; -	3.6×10^8; -
C (vector-tensor invers.)	8.1×10^7; 279	8.6×10^7; 313	1.4×10^8; 594	2.3×10^8; 660
D ($1/\sqrt{\mu}[x,y, x^2,y^2]$)	1.1×10^8; 276	1.4×10^8; 211	1.6×10^8; 554	2.5×10^8; 653
E ($1/\sqrt{\mu}[x,y, \rho^2]$)	8.9×10^7; 278	9.1×10^7; 257	1.2×10^8; 554	2.5×10^7; 653
G (inversion model)	-; 160*	-; 115*	-; 370*	-; 470*

*depths to top of models (not centroids)